Journal of Geophysical Research: Atmospheres

RESEARCH ARTICLE
10.1029/2018JD028579

The Relationships Between Cloud Top Radiative Cooling Rates, Surface Latent Heat Fluxes, and Cloud-Base Heights in Marine Stratocumulus

Youtong Zheng[1], Daniel Rosenfeld[2], and Zhanqing Li[1,3]

[1]Department of Atmospheric and Oceanic Science and Earth System Science Interdisciplinary Center, University of Maryland, College Park, MD, USA, [2]Institute of Earth Sciences, The Hebrew University of Jerusalem, Jerusalem, Israel, [3]State Key Laboratory of Earth Surface Processes and Resource Ecology, and College of Global Change and Earth System Science, Beijing Normal University, Beijing, China

Key Points:
- The vast majority of decoupled stratocumulus are coupled with the surfaces by cumulus convection in subtropical northeast Pacific
- Cloud top radiative cooling of stratocumulus regulates surface latent heat fluxes and cloud-base height in well-mixed boundary layers
- The strong surface forcing in cumulus-coupled boundary layers dominate the signature of the cloud top radiative cooling in influencing surface energetics

Supporting Information:
- Supporting Information S1

Correspondence to:
Y. Zheng,
zhengyoutong@gmail.com

Citation:
Zheng, Y., Rosenfeld, D., & Li, Z. (2018). The relationships between cloud top radiative cooling rates, surface latent heat fluxes, and cloud-base heights in marine stratocumulus. *Journal of Geophysical Research: Atmospheres*, *123*, 11,678–11,690. https://doi.org/10.1029/2018JD028579

Received 26 FEB 2018
Accepted 28 SEP 2018
Accepted article online 12 OCT 2018
Published online 30 OCT 2018

©2018. American Geophysical Union. All Rights Reserved.

Abstract Cloud top radiative cooling (CTRC) drives turbulence in marine boundary layers (MBLs) topped by stratocumulus clouds. This study examines the role of CTRC in regulating the surface-cloud coupling, surface latent heat fluxes, and cloud base height by exploiting a 6-month worth of shipborne observations over the subtropical northeast Pacific in combination with geostationary satellite data. We find that owning to the prevailing equatorward flow that advects stratocumulus clouds over warmer sea surfaces, the vast majority of the decoupled stratocumulus decks are fed by divergence from the tops of underlying cumulus, forming cumulus-coupled MBL. The cumulus-coupled and well-mixed MBL dominate the subtropical MBL regimes. We find that strong CTRC favors greater (smaller) occurrence frequency of well-mixed (cumulus-coupled) MBLs. In well-mixed MBLs, strong CTRC enhances entrainment of dry free-tropospheric air, desiccates the MBL, increases the surface latent heat fluxes, and elevates the cloud-base height. This is demonstrated by the observed covariabilities between the CTRC rate and surface latent heat fluxes and cloud-base height. The relationships are more statistically significant in conditions where the inversion strength is relatively weak, and thus, the entrainment is more effective. In cumulus-coupled MBLs, however, the influence of CTRC in regulating the surface moisture is not detected by the ship observations. The much greater latent heat fluxes than the CTRC rate in cumulus-coupled MBLs suggest stronger surface forcing, which substantially tames the footprint of CTRC.

1. Introduction

Marine stratocumulus (Sc) clouds markedly affect Earth's radiative balance because of their low altitudes and extensive cloud coverage (Hartmann et al., 1992; Hartmann & Short, 1980; Stephens, 2005; Stephens & Greenwald, 1991). The extensive solid cloud cover produces considerable infrared radiative cooling concentrated near cloud top, which is the dominant driving mechanism for convection under marine conditions (Caldwell et al., 2005; Lilly, 1968; Wood, 2012; Zheng et al., 2016). The convective mixing transports the moisture from sea surface to the Sc layer to prevent it from being dissipated by entrainment of dry free-tropospheric air. Thus, Sc favors a well-mixed boundary layer that is coupled with the sea surface for moisture supply by convective mixing.

Sc clouds are most prevalent over subtropical oceans where Sc cloud systems are advected from cold to warm sea surfaces. The progressively warmed sea surface deepens the Sc-topped boundary layer (STBL) and causes systematic decoupling of the STBL through cloud top entrainment feedback, a mechanism commonly known as *deepening-warming* decoupling (Bretherton & Wyant, 1997). Note that the term *coupling/decoupling* used here is for a planetary boundary layer, defined as the layer of air between the sea surface and the inversion that bounds the cloud tops, not for the cloud itself. A coupled STBL refers to a boundary layer that is well mixed, and any STBL that is not well mixed is defined as decoupled. However, the cold advection offers a conditionally unstable environment favorable for formations of cumulus (Cu) clouds that develop from the moist surface layer, shoot, and spread into the existing Sc decks while feeding their cloud water with the surface moisture (Martin et al., 1995; Miller & Albrecht, 1995). In this situation, the Cu-fed Sc is clearly coupled with the surface even though the boundary layer is often not well mixed. This Cu-fed Sc mechanism largely explains the abundance of persistent Sc decks in poorly mixed (stratified) marine boundary layers (Klein et al., 1995).

This study concerns with investigating the influences of cloud top radiative cooling (CTRC) on some key properties of a STBL, namely, surface-cloud coupling regime, surface heat fluxes, and cloud-base height. There are

two motivations for such a pursuit. First of all, the role of CTRC in regulating the surface energetics and cloud-base height via entrainment processes has been indicated by a recent large-eddy simulation study (Kazil et al., 2017), but robust observational evidences are still scant. Using 6 days of data collected at a cruise in the southeast Pacific, Caldwell et al. (2005) found a marked diurnal cycle of lifting condensation level (LCL) driven by CTRC via entrainment process. But, the robustness of their finding is limited by the scant amount of observations (6-day worth of data). Similar sampling size issue also exists in other conventional field campaign studies. The only long-term record of STBL observations is made, under the aegis of the U.S. Department of Energy (DOE) Atmospheric Radiation Measurement (ARM) Program, on the Graciosa Island in the northeast Atlantic (Wood et al., 2015), but the island effect precludes measurements of sea surface fluxes.

Second, although CTRC-driven diurnal behaviors of STBLs have been extensively observed (Caldwell et al., 2005; Fairall et al., 1990; Matsui et al., 2006; Nicholls, 1984; O'Dell et al., 2008; Painemal et al., 2012; Rahn & Garreaud, 2010; Tang & Zou, 2018; Wood et al., 2002; Wood et al., 2009; Zuidema & Hartmann, 1995) and modeled (Garreaud & Muñoz, 2004; Kazil et al., 2017; Stevens et al., 1998; Wyant et al., 2010), studies of these kinds with a focus on the Cu-coupled STBL have been lacking. Usually, emergence of the Cu-coupled STBL itself is considered as a part of the diurnal cycle. However, lifetime of the Cu-fed Sc is usually adequately long (several tens of hours) to be exposed to a full cycle of solar-driven influences. Thus, it is necessary to study their diurnal behavior in isolation. Observational studies of Cu-fed Sc are exclusively limited to the Atlantic Stratocumulus Transition Experiment (ATEX) field campaign (Albrecht et al., 1995). The number of samples, again, is limited. An investigation by Klein et al. (1995) that uses a larger population of observations, however, is significantly limited by ill-prepared instrumentations.

The Marine ARM (Atmospheric Radiation Measurement) GPCI (Global Energy and Water Cycle Experiment-Cloud System Study-Pacific Cross-section Intercomparison) Investigation of Clouds (MAGIC) field campaign (Lewis & Teixeira, 2015; Zhou et al., 2015) in the northeast Pacific deploys a series of state-of-the-art passive and active instruments with unprecedentedly long (6-month) ship-borne observations of marine clouds. This allows statistic-based evaluation of the influence of CTRC on the surface energetics in both well-mixed and Cu-coupled STBLs. Objectives of this study are twofold:

(1). Examine the role of CTRC in controlling the surface-Sc coupling, surface heat fluxes, and cloud-base height using 6-month MAGIC observations.
(2). Compare the results between well-mixed and Cu-coupled STBLs.

2. Revisiting the Classification of Coupling State

As mentioned above, the conventional definition of *coupling* is based on the extent to which a marine boundary layer is well mixed. Based on this definition, it has been a common practice to classify STBLs into coupled (well mixed) and decoupled (not well mixed) STBLs (Dong et al., 2015; Jones et al., 2011; Zheng et al., 2016). Such a classification scheme fails to distinguish between two apparently different types of STBL: Cu-coupled STBL and decoupled STBL without Cu feedings. Neither of these two types of STBL are well mixed, but whether the Sc deck is fed by Cu convection certainly makes a difference to the cloud microstructure and macrostructure, cloud evolution, and boundary layer turbulence, as indicated in earlier studies (Goren et al., 2018; Martin et al., 1995; Miller & Albrecht, 1995). Furthermore, the ambient low-level temperature advections, with which these two different STBL regimes are associated, are rather different. When Sc decks are advected over progressively warmer water (low-level cold-advection conditions), they tend to become decoupled due to the deepening-warming mechanism (Bretherton & Wyant, 1997). The warmed sea surface temperature (SST) deepens the STBL, via entrainment feedbacks, and stratifies the boundary layer, separating the Sc-containing layer from the surface mixed layer. Such a structure with two separated layers usually does not persist. Due to the low-level cold temperature advection, the subcloud layer is often conditionally unstable, which is conducive for the newly formed Cu clouds to penetrate through the subcloud layer, forming a Cu-coupled SBTL (Figure 1a). Under warm advection conditions, however, the subcloud layer is stabilized to the extent that the Cu penetration is substantially suppressed (Figure 1b). Such a shutdown of Cu feeding can markedly prolong the lifetime of decoupled Sc decks (Goren et al., 2018) by reducing the tendency for precipitation-induced breakup of Sc decks. On the contrary, Sc decks in a Cu-fed STBL are more likely to breakup due to locally enhanced entrainment by vigorous Cu convection (Xiao et al., 2011). Such

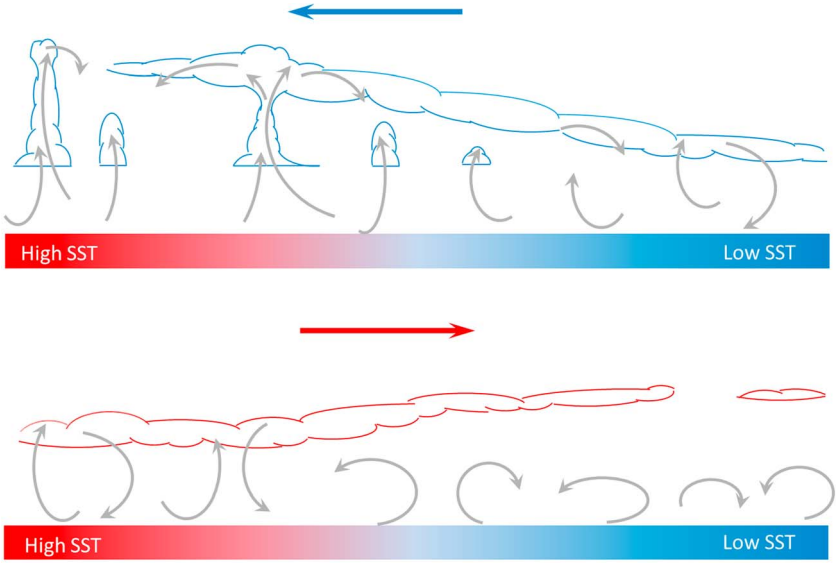


Figure 1. Cartoon illustrating the effect of low-level temperature advection on the coupling state of stratocumulus clouds.

a distinction in behaviors of Sc decks in the two STBL regimes stresses the need for distinguishing between the decoupled STBLs with and without Cu feedings.

In this study, we start with classifying Sc decks into those with and without Cu feedings (single-layer Sc versus Cu-fed Sc). As will be shown latter, the vast majority of single-layer Sc observed during the MAGIC field campaign are coupled, and the decoupled Sc deck without Cu feedings is a marginal category. This reflects ubiquitous presences of Cu convection after Sc becomes decoupled. The frequent occurrence of Cu-coupled STBLs during the MAGIC offers us an excellent opportunity to statistically compare the roles of CTRC in modulating STBL properties between Cu-coupled and well-mixed STBLs. Such an attempt, to our knowledge, has never been undertaken before.

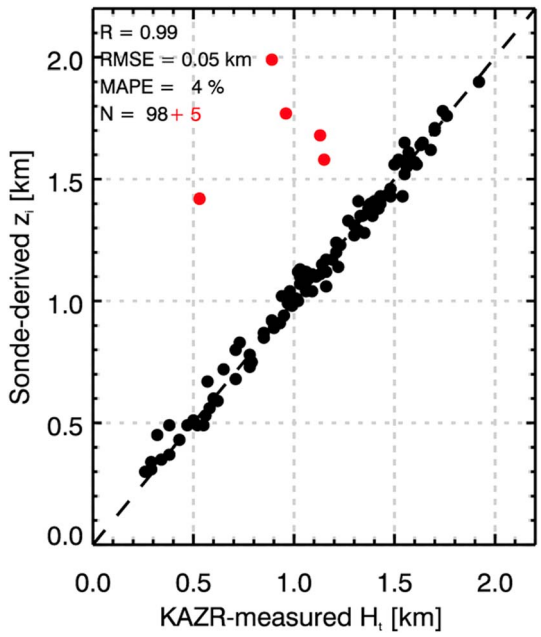


Figure 2. Comparison between the Ka-band ARM Zenith Radar (KAZR)-measured mean cloud top height (H_t) and sounding-derived altitude of inversion layer base (z_i). The excluded cases are marked by red points. The correlation coefficient (R), root-mean-square-error (RMSE), mean-average-percentage-error (MAPE), and number of cases (N) are provided.

The next section introduces the satellite and shipborne observations made during the MAGIC and the methodology of classifying STBL regimes. Section 4 presents the results, followed by conclusions given in section 5.

3. Methodology

We use the ship-based observations made during the MAGIC field campaign, which has 6-month worth of data (October to December 2012; June to August 2013) acquired by a large array of instruments assembled by the ARM program. Ship-based measurements were collected along an ~4,100 km ship transect from the Los Angeles (33.7°N, 118.2°W) to the Honolulu in Hawaii (21.3°N, 157.8°W). The DOE/ARM Mobile Facility 2 (AMF2) was deployed on the commercial ship *Horizon Spirit*. A Vaisala Ceilometer is used to measure cloud-base height. Heavy precipitation could distort ceilometer measurements, but since precipitation in overcast warm clouds mostly occurs in the form of drizzle (Leon et al., 2008), the distortion is expected to be small. The marine meteorological measurement (MARMET) data sets provide standard surface meteorological parameters such as air temperature, dew point temperature, pressure, relative humidity, wind speed, and SST (Zhou et al., 2015). We calculate the LCL using Espy's equation (Bohren & Albrecht, 1998), and the uncertainty is approximately 1% under atmospheric condition over the subtropical ocean (Lawrence, 2005). The Marine Flux data set (MARFLUX) offers surface

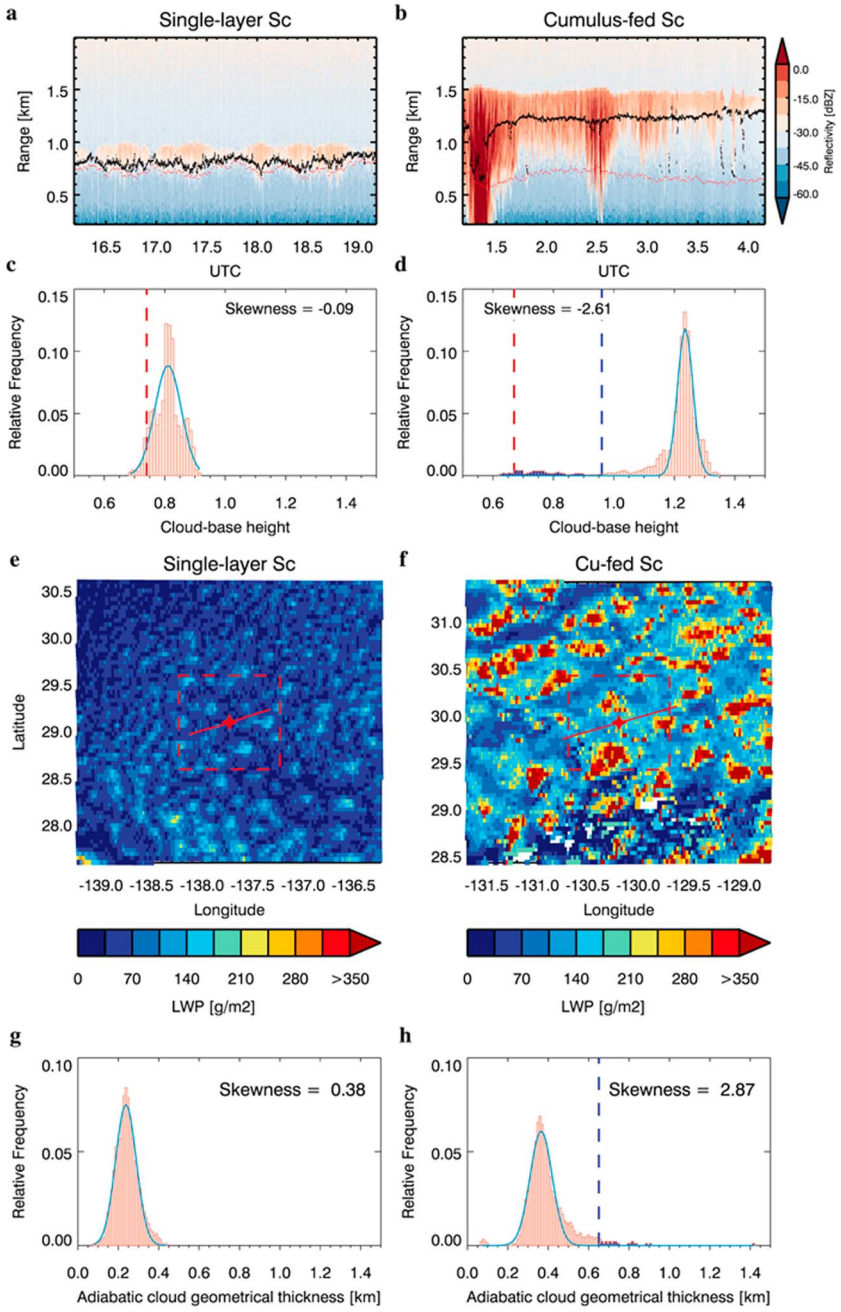


Figure 3. Example cases of single-layer (left panel) and Cu-fed Sc (right panel). (a and b) Time-height plots of Ka-band ARM Zenith Radar reflectivity. The black and red points stand for the ceilometer-measured cloud base heights and lifting condensation levels, respectively. (c and d) Probability density function of ceilometer-derived cloud-base heights. The vertical red dashed lines represent the mean lifting condensation level during the 3-hr segment. The light blue solid lines are the Gaussian-fit lines. In (d), the vertical dashed blue lines mark the reference altitude (median value minus two standard deviations), below which the measurements (blue bins) are identified as *outliers*. (e and f) 2-D view of the GOES-derived liquid water path. The dashed rectangles mark the 1° × 1° sampling regions centered on the ship locations marked by red stars. The red lines denote the ship tracks during the courses of 3 hr. (g and h) Probability density function of GOES-derived CGT_a. In (h), the vertical dashed line marks the median value plus two standard deviation of CGT_a. The dates for the two example cases are 3 June 2013 (left panel) and 9 July 2013 (right panel).

latent heat fluxes (LHFs), which are calculated based on moisture difference between sea surface and near-surface air, and surface wind speed (Fairall et al., 1996). Balloon-based radiosonde data provide vertical profiles of thermodynamic parameters. To determine the strength of inversion, we define the inversion

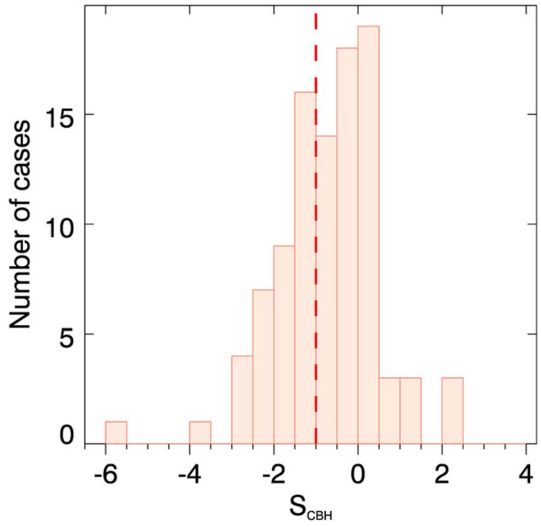


Figure 4. Distribution of S_{CBH} for all the cases surveyed. The red dashed line marks the threshold value selected for separating single-layer and Cu-fed Sc clouds.

layer as the layer where the vertical temperature gradient (dT/dz) is positive and its layer-mean value is the greatest below the 3-km level. The strength of the inversion is approximated by the temperature contrast (ΔT_{inv}) between the inversion-layer base (z_i) and the top of the inversion layer. We use the 35-GHz Ka-band ARM Zenith Radar (KAZR) to detect cloud boundaries. Following Zheng et al. (2016), we use the radar-measured cloud boundaries and radiosonde-observed vertical profiles of temperature and moisture as input for the discreet ordinate radiative transfer (DISTORT) model and compute the CTRC by integrating the modeled heating rate (longwave + shortwave) throughout the Sc cloud layer.

In addition to the MAGIC ship-based measurements, the 15th Geostationary Operational Environmental Satellite (GOES-15) cloud parameter data from National Aeronautics and Space Administration (NASA) Langley Research Center cloud products (http://www-angler.larc.nasa.gov) were used. The data are sampled at 4 × 4 km horizontal resolution every 30 min. Cloud quantities used in this study are cloud top temperature, cloud visible optical depth, (τ) and cloud droplet effective radius (r_e), which are retrieved by visible infrared solar infrared split-window technique (Minnis et al., 1995) from the multispectral GOES imager data. Liquid water path (LWP) is estimated as LWP = (2/3).r_e.τ. We derive the adiabatic cloud geometrical thickness (CGT_a) by $CGT_a = (2LWP/c_w)^{1/2}$, in which c_w, the vertical variation of the adiabatic liquid water mixing ratio with height, is a weak function of temperature and pressure (Albrecht et al., 1990) and we simply use the value of 2 g · m^{-3} · km^{-1} that is typical for marine warm clouds.

3.1. Case Selection

A total of 103 overcast STBL cases with warm cloud cover within 1° × 1° area larger than 90% are selected by the GOES-15 data. Each case represents a 1° × 1° satellite scene centered on the ship location. Since the ship speed is ~30 km/hr, we select 3-hr ship measurements that covered a distance of ~ 90 km, comparable to the horizontal size of a 1° × 1° satellite scene. Each satellite scene was selected at radiosonde launch times (4 times per day) because the radiosondes were launched every 6 hr, allowing the ship to travel sufficiently long distance to avoid overlap sampling between two consecutive scenes. A comparison between the radiosonde-derived z_i and KAZR-derived mean cloud top height (H_t) shows overall good agreement (Figure 2). There are five outliers with z_i much higher than H_t. Examining their KAZR reflectivity images reveals a collapsing STBL with a considerable portion of Sc decks already dissipated (Figure S1). Since this study focuses on steady state STBLs, those five cases are excluded from analysis. Despite the exclusions, bulk of the cases (98 out of 103) are kept, which have overcast solid Sc decks that generate CTRC to initiate a series of feedback to maintain a steady STBL. This steady system manifests itself as the excellent agreement between z_i and H_t (R = 0.99 in Figure 2).

Table 1
Comparison of Key Parameters of STBL Between Single-Layer and Cu-Fed Sc Clouds

	Well-mixed STBL	Cu-coupled STBL
Longitude (° W)	126.4 ± 6.4	134.0 ± 6.0
S_{CBH}	0.09 ± 0.82	−1.91 ± 0.84
SST (K)	291.5 ± 2.0	294.0 ± 1.8
z_i (km)	0.83 ± 0.33	1.37 ± 0.23
ΔT_{inv} (K)	8.58 ± 3.47	6.92 ± 2.01
LWP (g/m^2)	70.8 ± 48.7	91.6 ± 50.6
LCL (km)	0.48 ± 0.28	0.68 ± 0.16
LHF (W/m^2)	93.4 ± 39.5	119.1 ± 40.3
CTRC (W/m^2)	82.1 ± 25.8	83.6 ± 22.4
θ_{CBH}-θ_{surf} (K)	0.25 ± 0.32	1.02 ± 0.69

Note. θ_{CBH}-θ_{surf} represents the potential temperature difference between the bases of Sc decks and the surfaces.

3.2. Cloud Regime Identification

During each 3-hr segment, we use the skewness of the ceilometer-measured cloud-base height (S_{CBH}), in combination with the KAZR reflectivity image, to differentiate the single-layer and Cu-fed Sc. This method is based on the fact that the probability density function (PDF) of cloud-base height for Sc decks typically follows a normal distribution (Wood & Taylor, 2001) and the occurrence of underlying scattered Cu clouds makes the PDF negatively skewed. This is illustrated in Figure 3, which shows examples of single-layer and Cu-fed Sc from ship- and satellite-based observations. The KAZR reflectivity image of single-layer Sc (Figure 3a) presents coupled Sc decks with cloud bases close to LCL calculated from the temperatures measured at ~20 m above sea level (ASL). The PDF of ceilometer-measured cloud-base height (Figure 3c) shows a narrow width (from ~0.7 to ~0.9 km), which has a small value of S_{CBH}. The Cu-fed Sc case,

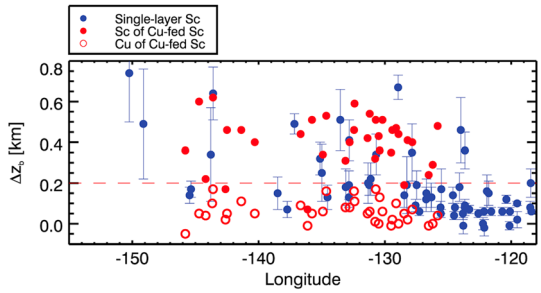


Figure 5. Longitudinal distribution of coupling state for selected cases. The red dashed line marks the threshold value selected for separating coupled and decoupled cloud elements.

however, reveals a markedly negatively skewed PDF (S_{CBH} = −2.61; Figure 3d) with a noticeable amount of cloud-base height measurements much lower than the median value. These low cloud bases, as shown by the KAZR reflectivity image of Figure 3b, correspond to the scattered Cu clouds underlying the Sc decks. These Cu clouds' bases are close to LCL, indicating that they are developed from moist surface layer. Some cumuli have already developed so appreciably that they penetrate into the overlying Sc decks. The penetration causes thickened clouds with more drizzling and cloud tops higher than the surroundings. The *Cu-fed* feature is also clearly seen in GOES images (Figure 3f) where patches of cloud elements have much higher values of LWP than the surroundings. In contrast, the LWP distribution of the single-layer Sc is markedly less variable. The PDFs of derived CGT_a mimics the PDFs of ceilometer-measured cloud-base height (Figures 3e–3h). The range of CGT_a variability for the single-layer Sc is narrow (Figure 3g), whereas the CGT_a PDF of the Cu-fed Sc is markedly skewed in an opposite direction (Figure 3h) because deeper clouds have lower cloud bases under the same cloud tops.

Figure 4a shows the histogram of S_{CBH} for all the 98 cases. A large portion of cases are not skewed ($-0.5 < S_{CBH} < 0.5$). This is consistent with the conventional wisdom that overcast low clouds are associated with Gaussian-distributed cloud-base height (Considine et al., 1997). Here we use a S_{CBH} threshold of −1 to separate the single-layer and Cu-fed Sc clouds. The primary reason for this threshold value is that the mean value of S_{CBH} for cases with S_{CBH} greater than −1 is around 0 (Table 1), consistent with the idea that single-layer Sc clouds should be nonskewed. Visual examinations of KAZR reflectivity images for all the 98 cases further encourages the use of S_{CBH} threshold of −1 to differentiate between the single-layer and Cu-fed Sc. The main results drawn in this study is not sensitive to this threshold value.

Figure 5 shows the longitudinal distribution of the coupling state for selected cases. For single-layer Sc cases, we use the mean difference between cloud-base height and LCL during a 3-hr segment (Δz_b) as the measure of coupling (Jones et al., 2011). For Cu-fed Sc clouds, we calculate the Δz_b for both the Cu and Sc components. In order to extract the Cu clouds measurements, we assume that randomly distributed Cu clouds with low cloud bases are outliers, which deviate markedly from the cloud bases of Sc decks that typically follows a normal distribution (Figure 3d). Thus, we statistically select Cu clouds measurements by identifying cloud-base heights lower than the median value by two standard deviations (vertical blue dashed line in Figure 3d), leaving the remained measurements to be the Sc decks. This rough classification procedure is able to separate the bulk of the measurements but may not accurately classify cloud elements in the transition between the Cu clouds and the Sc decks. To minimize the effect of misclassifications, for Sc decks, we simply use the median value of the classified cloud-base height measurements to calculate the Δz_b. For Cu clouds, the lowest 10% of the extracted Cu cloud-base heights were used to compute the Δz_b for excluding the artificially higher cloud bases caused by Cu tilting or possible misclassifications (Figure 3b). A threshold of 0.2 km is used to differentiate the coupled and decoupled clouds, which is slightly higher than the 0.15 km used by Jones et al. (2011). The reason is that Jones et al. (2011) calculated the LCL from the temperatures measured at ~150 m ASL, which is higher than the altitude of temperature measurements (~20 m ASL) in this study. Thus, we tend to underestimate the LCL due to the fact that surface-layer air parcels are less representative of the air parcels associated with convective cloud development than mixed-layer air parcels (Craven et al., 2002).

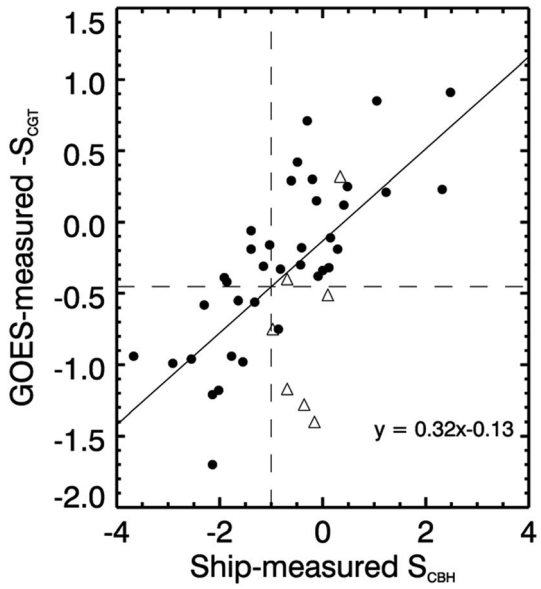


Figure 6. Comparison between S_{CBH} and $-S_{CGT}$. The upward triangles mark the decoupled single-layer Sc clouds identified by ship-borne measurements. The dashed lines represent the thresholds of decoupling.

There are three noteworthy features in Figure 5. First of all, there is a systematic offshore decoupling of Sc decks. The coastal regions are dominated by coupled Sc decks on top of well-mixed marine boundary layers, whereas stratified STBLs associated with decoupled single-layer Sc and

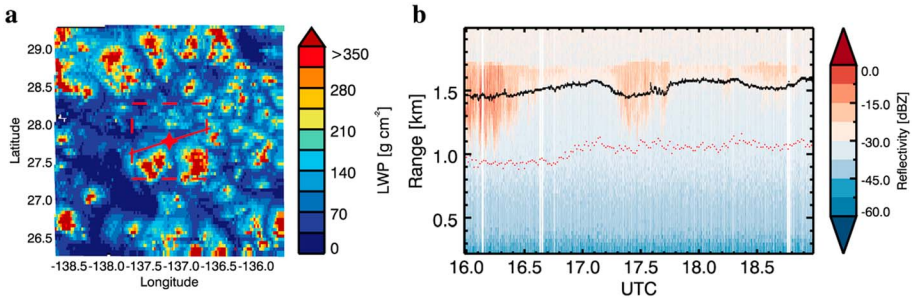


Figure 7. Example case for a Cu-fed Sc in which the ship fails the sample the Cu clouds. (a) Time-height plots of Ka-band ARM Zenith Radar reflectivity. The black and red points stand for the ceilometer-measured cloud base heights and lifting condensation levels, respectively. (b) The 2-D view of the GOES-derived liquid water path (LWP). The dashed rectangles mark the 1° × 1° sampling regions centered on the ship location marked by red stars. The red line denotes the ship track during the three-hour courses.

Cu-fed Sc regimes occur more frequently in downstream regions. Second, the Sc decks in Cu-coupled STBLs are mostly decoupled (red solid circles), while the Cu components are coupled (red open circles).

Third, Δz_b of the decoupled single-layer Sc shows larger variability (larger error bar) during a 3-hr segment than the coupled single-layer Sc. This indicates that these decoupled single-layer Sc decks are not uniformly decoupled but have relatively more coupled components. The coupled fraction during the 3-hr ship measurements is not adequate for the S_{CBH} value to be negative enough for meeting the criteria of Cu-fed Sc definition. Note that a ship moving along a path can only offer one-dimensional sampling of clouds in a two-dimensional (2-D) cloud filed. Given that Cu clouds in a Cu-fed Sc system are randomly scattered around, it is possible that the ship happens to miss most of the Cu-fed Sc elements along its track during a 3-hr period. This may cause a Cu-fed Sc regime to be misclassified as decoupled single-layer Sc. To examine this hypothesis, we survey the GOES-15 satellite data because the large-scale satellite images offer a more complete sampling of Sc decks. To mitigate known problems for LWP retrieval in conditions with low solar zenith angle, we selected cases with solar zenith angle smaller than 70° and compute their CGT_a skewness (S_{CGT}) within a 1° × 1° satellite scene centered on the ship location. A comparison between the ship-measured S_{CBH} and the opposite of the S_{CGT} shows an overall agreement (Figure 6). A least squares fit suggests that a S_{CBH} threshold of -1 corresponds to $-S_{CGT}$ of -0.45. The reason for less skewed CGT_a is that the resolution of GOES retrievals is 4 km, which is coarser than that of ceilometers. Thus, the averaged CGT_a in a 4-km pixel tends to underestimate the geometrical thickness of the most active Cu clouds with sizes smaller than 4 km, leading to less skewed PDFs. There, however, are some exceptions, in which cases satellite data identify them as Cu-fed Sc ($-S_{CGT} < -0.45$), whereas the corresponding S_{CBH} has smaller absolute values. This is likely attributed to the sampling limitation of ship-based measurements, which unfortunately miss the scarcely distributed Cu clouds and only capture the decoupled Sc decks. Examining the decoupled single-layer Sc identified by ship measurements (open upward triangles) confirms this hypothesis as five out of the seven ship-identified decoupled single-layer Sc cases are classified as Cu-fed Sc by GOES data. Figure 7 shows an example of such case. The ship track (red solid line in Figure 7b) happens to miss all the high-LWP cloud cells and only samples the decoupled Sc anvils as shown in the radar image. This suggests that the already scant cases of decoupled single-layer Sc (16 out of 98), identified by ship-borne measurements, stand a high chance to be decoupled Sc decks in Cu-fed Sc regimes.

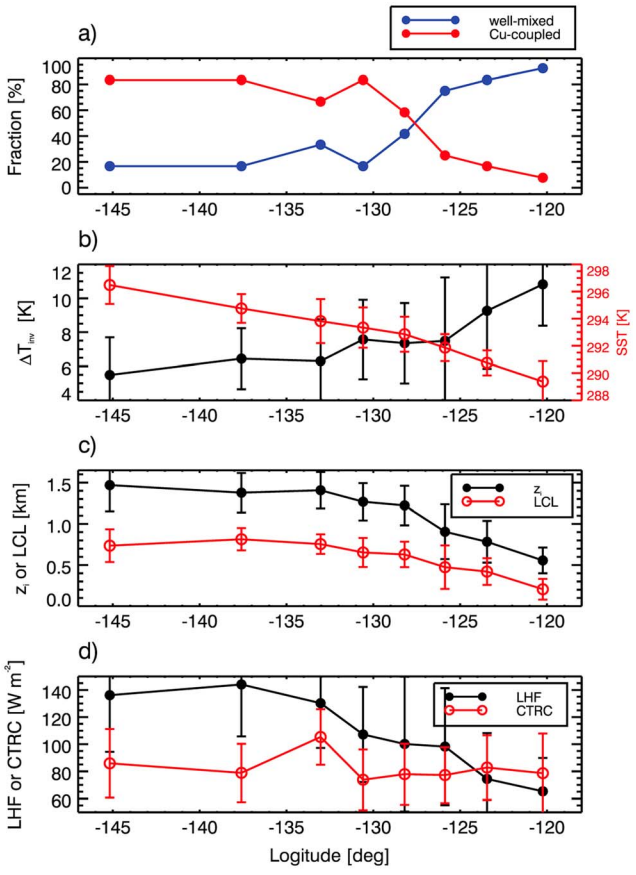


Figure 8. Longitudinal variations of key stratocumulus-topped boundary layer parameters. The 98 cases are divided into eight equal-size bins.

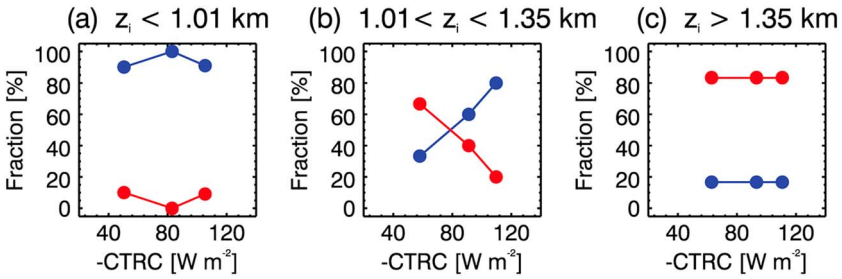


Figure 9. Variations of fraction of well-mixed (blue) and Cu-coupled stratocumulus-topped boundary layers (red) with 4-hr-lag cloud top radiative cooling (CTRC) for (a) $z_i < 1.01$ km, (b) $1.01 < z_i < 1.35$ km, and (c) $z_i > 1.35$ km. In each figure, samples are divided into three equal-size bins, each having 10 or 11 samples.

The above analysis suggests that decoupled Sc without Cu feedings is a marginal category over the subtropical northeast Pacific. The prevailing cold advections offer a conditionally unstable thermodynamic setting conducive for the formation of Cu-fed Sc regimes. In the remainder of this paper, we concern ourselves with coupled single-layer Sc and Cu-fed Sc, which are associated with well-mixed and Cu-coupled STBLs, respectively. Table 1 compares some key STBL parameters between these two types of STBL regime.

Cu-fed Sc clouds are more distant from California with warmer SST, deeper boundary layer, and weaker inversion. The weaker inversion is favorable for more efficient entrainment of dry free-tropospheric air (Deardorff, 1980). This desiccates the boundary layer, elevates the LCL, and enhances the LHF. The occurrence of active cumulus towers, which are usually deep and precipitating (Stevens et al., 1998), causes higher LWP in Cu-coupled STBLs than the well-mixed STBLs. There is no statistically significant difference in CTRC between these two cloud types.

4. Results

We will first revisit the large-scale meteorological control upon the STBLs before focusing on the role of CTRC. The reason is that all of the key STBL variables to be examined in this study (surface fluxes, cloud-base heights, and coupling state) are affected by the large-scale dynamics with various degrees (Wood, 2012). It is thus necessary to evaluate the influences of large-scale state for better constraining the role of CTRC.

4.1. Offshore Decoupling of STBL as Explained by Large-Scale Dynamics

The most distinct cloud climatology over the subtropical oceans is the offshore decoupling of STBLs. As discussed in section 3, such a phenomenology is primarily driven by the large-scale advections of coastal Sc decks to progressively warmer SST through entrainment feedback (Bretherton & Wyant, 1997). Figure 8 shows the longitudinal variations of the occurrence of coupled/decoupled STBLs and some key STBL and large-scale variables. The key features predicted by the deepening-warming decoupling mechanism (Bretherton & Wyant, 1997) are revealed in our observational data (Figure 8): warmer SST, deeper boundary

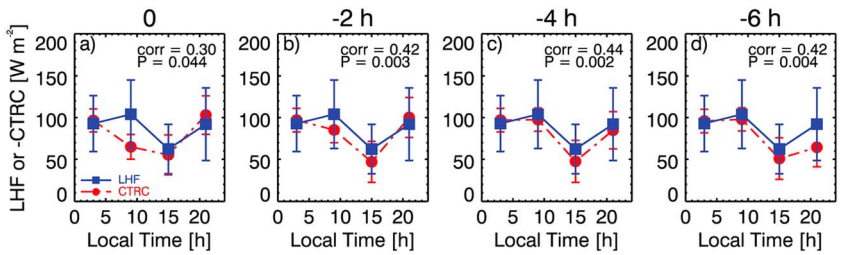


Figure 10. Diurnal variations of LHF (blue) and –CTRC (red). The error bars mark the standard deviations of samples in each bin. The correlation coefficient and *p*-value are calculated based on samples with each representing 3-hr measurements. Figures from left to right correspond to the sets in which CTRC is calculated at 0, 2, 4, and 6 hr prior to the time of each case. The number of samples for the 15 LST bin (five samples) is fewer than those of other local times (12–17 samples) because of the insolation-induced decoupling.

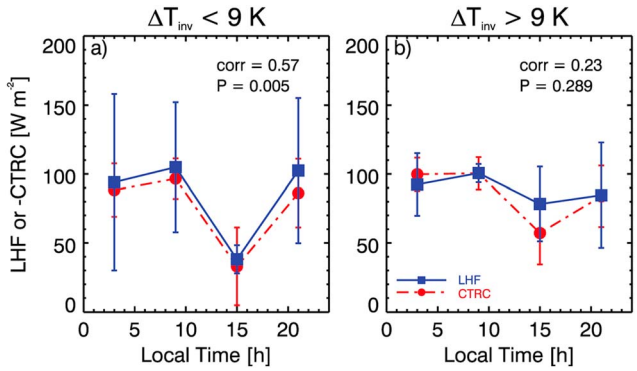


Figure 11. Same to Figure 10 but samples are divided for $\Delta T_{inv} < 9$ K and $\Delta T_{inv} > 9$ K.

layer, weaker inversion, greater latent heat fluxes (LHFs), and less frequent occurrence of well-mixed STBLs in downstream remote oceans relative to upstream coastal regions. The marked offshore increase of LHF is particularly noteworthy. According to the deepening-warming theory, an increasing dominance of LHF in boundary layer energetics is the key driving factor of the systematic stratification of STBLs (Bretherton & Wyant, 1997). Such an offshore enhancement of LHF, however, has not been observed in the previous study using MAGIC data (Zhou et al., 2015). The inconsistency is likely due to the different sampling strategies. This study focuses upon overcast STBLs, while Zhou et al. (2015) sample cases across the full spectrum of cloud fractional coverages. The deepening-warming theory is derived from the mixed-layer model (Lilly, 1968) that assumes a dominance of CTRC. Such an assumption is only valid in full cloudy conditions in which the extensive solid Sc decks generate sufficient amount of CTRC for sustaining the feedback between the convective circulations, LHF, and entrainment. The increased LHF is the result of the radiation-turbulence-entrainment feedback, the strength of which is weak in low-cloudy conditions where the domain-integrated CTRC rate is low. We conclude here that MAGIC observations are consistent with the Bretherton and Wyant's (1997) hypothesis that LHF plays an important role in promoting the systematic offshore stratification of STBLs.

It is noteworthy that there is no detectable longitudinal trend of CTRC. This indicates that the longitudinal variation of free-tropospheric moisture (Zhou et al., 2015) has little effect on modulating the CTRC. This motivates us to focus on the diurnal time scale at which the insolation-modulated variation of CTRC is significant (Zheng et al., 2016).

4.2. Effects of CTRC on the Coupling State

We have observed the role of large-scale dynamics in driving the offshore decoupling. To tease out the signature of CTRC from the large-scale dynamics, we divide the cases into three equal-sized groups according to z_i. We use z_i because it has been considered as one of the most important variables dictating the coupling state of STBL in the theoretical framework of deepening-warming mechanism (Wood & Bretherton, 2004; Zuidema et al., 2009). Figure 9 shows the occurrence frequency of well-mixed STBLs (blue) and Cu-coupled STBLs (red) as a function of CTRC for the three equal-size groups. The CTRC is calculated 4 hr prior to the observational time of each case because the boundary layer requires several hours to adjust its coupling state to the radiative forcing (the selection of 4-hr will be discussed latter). We find that the occurrence fraction is independent of CTRC in shallow- and deep-z_i groups. When STBL is shallow ($z_i < 1.01$ km in this study), the vast majority of STBLs are well mixed, whereas stratified STBLs become more dominant in deep STBLs. This result is consistent with earlier studies (Wood & Bretherton, 2004; Zuidema et al., 2009), confirming the more significant role of z_i, relative to the CTRC, in determining the coupling state of STBLs. For medium-z_i group, however, the response of the coupling state to CTRC becomes marked; stronger CTRC is associated with greater fraction of well-mixed STBLs and vice versa. The sensitivity is considerable (~10% per 10 W/m^2). This result is consistent with the idea that weakened convection induced by reduction in CTRC leads to a less well-mixed STBL (Nicholls, 1984). Such an effect of CTRC, however, is conditioned by z_i. Only when the z_i is neither too deep nor too shallow that the CTRC-induced modification to the coupling state is present.

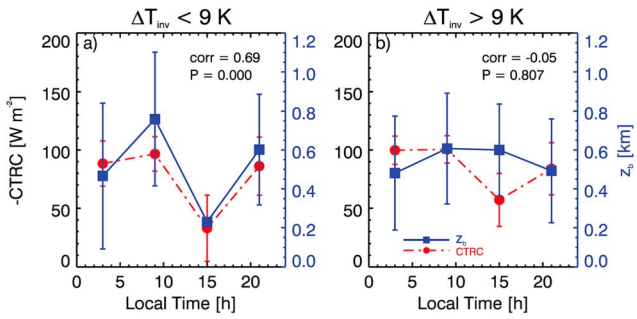


Figure 12. Same to Figure 11 but blue points represent cloud-base height.

4.3. Effects of CTRC on Surface Fluxes and Cloud-Base Height

Figure 10a shows the diurnal cycles of CTRC and LHF for well-mixed STBL cases. A marked time lag between the CTRC and LHF is noted. Starting from sunrise, absorption of incoming solar radiation warms cloud tops and weakens the CTRC (3–9 hr local time in Figure 10a), which decreases turbulence and cloud top entrainment. The reduced entrainment of free-tropospheric dry air, however, does not immediately moisten the surface air. From Figure 10a, the signature of CTRC-induced moistening starts to emerge after late morning, as seen from the reduced LHF from 9 to 15 local standard time (LST). To examine the time lag, we compute the CTRC 2/4/

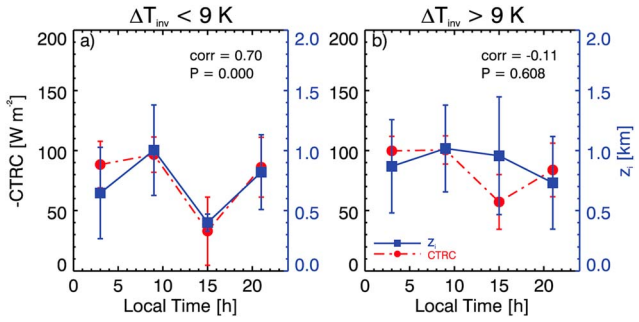


Figure 13. Same to Figure 11 but blue points represent inversion-layer height.

6 hr prior to the observational time for each case. These computed CTRCs could be intuitively interpreted as the footprints of CTRC from preceding hours. The comparisons between the diurnal cycles of LHF and the footprints of CTRC (Figures 10b–10d) dictate that time scales for the response of LHF to CTRC is ~4 hr although the 2- and 6-hr time lags show comparable CTRC-LHF correlations. This is consistent with the recent LES study (Kazil et al., 2017) that shows similar time-lag of LHF response to CTRC. We will use the 4-hr-lag CTRC throughout. The major conclusions drawn in this study is not sensitive to the selection of time lag.

This result confirms the role of CTRC in regulating the LHF as mentioned in section 4.1. This regulation is through the cloud top entrainment, the strength of which is influenced not only by the CTRC-produced turbulence but also the strength of the inversion. Stronger inversion suppresses the entrainment process and, thus, tames the footprint of CTRC in regulating the LHF. To examine the effect of inversion strength, we use the radiosonde-derived ΔT_{inv} to approximate the inversion strength and divide the cases in Figure 10c into two equally sized groups according to the ΔT_{inv}. A significant distinction between the two groups is noted. There is a much greater diurnal variability of LHF in week-inversion conditions ($\Delta T_{inv} < 9$ K) than the strong-inversion ones. Such a larger diurnal cycle is partially due to the greater CTRC variability in weak-inversion samples. But the more important factor driving the larger LHF variability is the greater sensitivity of LHF to CTRC in weak-inversion conditions that favor more efficient entrainment. This could be supported by the fact that LHF and CTRC covaries by almost the same amplitude in the weak-inversion group (Figure 11a) whereas amplitude for LHF variation is much smaller than CTRC in strong-inversion samples (Figure 11b).

In addition to LHF, cloud-base height (z_b) also adjusts, in a similar way, to the CTRC-induced STBL desiccation (Figure 12). Compared with LHF, it appears that the z_b is more dependent on the inversion strength. When the inversion is strong enough, there is no correlation between the CTRC and z_b at all (Figure 12b). The CTRC-z_b association is consistent with a previously observed linear relationship between z_b and cloud-base updrafts for marine low clouds (Zheng & Rosenfeld, 2015).

The entrainment influences not only the budget of moisture but also the budget of mass. Stronger entrainment deepens the boundary layer against the suppression from the large-scale subsidence. This is reflected by the diurnal variation of z_i (Figure 13) that is in sync with the z_b. The inversion layer strength regulates the amplitude of diurnal cycle of z_i as much as it regulates that of z_b. This indicates limited diurnal variations of cloud geometrical thickness and LWP for well-mixed STBLs. The CTRC-generated convection could both moisten and desiccate the boundary layer by increasing moisture fluxes and by enhancing the entrainment drying, respectively. As a result, the cloud geometrical thickness varies little.

For Cu-fed Sc cases, only 4 out of the 35 cases have the ΔT_{inv} greater than 9 K. Analysis of the group of samples with $\Delta T_{inv} < 9$ K shows no marked signal of CTRC in enhancing the LHF and in elevating cumulus base height (Figures 14a and 14b). There is even a slight negative correlation between CTRC and LHF. This is probably due to the moistening effect of precipitation, the intensity of which increases with convection intensity. This mechanism is more evident in Cu-coupled STBLs because the precipitation from the deep Cu clouds can often reach the surfaces, whereas drizzles in relatively shallower well-mixed STBLs are more likely to be evaporated in subcloud layers.

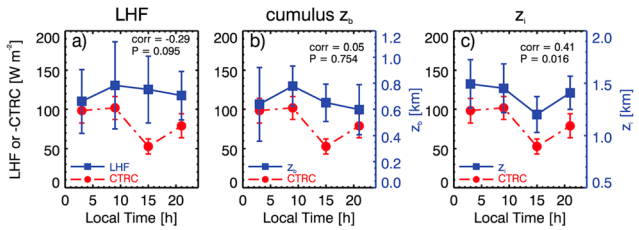


Figure 14. Diurnal variations of cloud top radiative cooling (CTRC; red), (a) latent heat flux (LHF), (b) Cu cloud-base height, and (c) inversion base height for Cu-coupled stratocumulus-topped boundary layers.

In general, the entrainment drying associated with the CTRC has negligible impacts on surface moisture in Cu-coupled STBLs at the diurnal time scale. This is in contrast to well-mixed STBLs in which the signature of CTRC in changing the surface moisture is much clearer (Figures 11a and 12a). Such a distinction in CTRC signature reflects the different degree of forcing from the sea surface. The Cu-coupled STBLs frequently occur in high-SST regions (Figure 5) where the surface forcing tends to be strong. This could be reflected by the markedly greater LHF than CTRC in Figure 14a, whereas

these two quantities are close in value in well-mixed STBLs (Figure 10). The greater influence of surface forcing inevitably weakens the signature of the CTRC in regulating boundary layer energetics.

The consideration of relative importance of surface- and CTRC-induced forcing leads to an interesting question: will the CTRC exerts detectable influences on the LHF in Cu-coupled STBLs if there is a weak low-level temperature advection (or weak surface forcing)? The observations used in this study are not adequate for addressing this question without the help of numerical simulations. Performing modeling analysis is beyond the scope of this study. Here we attempt to offer some hints for this question by using the MAGIC data. As was discussed, the key process linking the CTRC with the surface energetics is the entrainment, which regulates not only LHF but also the z_i. Unlike the LHF that is affected by both the entrainment and the surface forcing, the z_i is dominantly controlled by the entrainment when the large-scale subsidence varies little, which is the case at diurnal time scale (Eastman et al., 2016; Painemal et al., 2017). Thus, the diurnal variation of z_i should convey important information pertaining to the entrainment strength. Figure 14c shows a statistically significant covariability between the CTRC and the z_i in Cu-coupled STBLs. This suggests that the entrainment still plays an important role in the evolution of Cu-coupled STBLs despite that its signature on surface energetics is weakened by the advection-induced convection. Therefore, it is reasonable to hypothesize that changes in CTRC should modulate the surface energetics in Cu-coupled STBLs in the absence of low-level temperature advection. The time scale at which such a hypothesized CTRC effect is detectable in Cu-coupled STBLs is expected to be greater than 4 hr (as is for well-mixed STBLs) because of the greater depth of the Cu-coupled STBL. Moreover, the entrainment efficiency in Cu-coupled STBLs is likely to be lower than that in well-mixed STBLs as seen from the magnitude of z_i diurnal cycle (~0.3 km) being smaller than that of well-mixed STBLs (~0.6 km). As shown in Table 1, the subcloud layer in Cu-coupled SBLTs has a greater stability than the well-mixed STBLs. The more stable subcloud layer suppresses turbulence and thus entrainment. Note that in a local scale the cumulus convections are still vigorous enough to enhance the local entrainment. But the cumulus convections are intermittent (Figure 3b) and local (Figure 7b). A large fraction of the cloud field are quiescent Sc anvils (Figure 7) with low turbulence levels (Wood et al., 2018; Zheng et al., 2016). The weak turbulence suppresses vertical mixing as far as the domain-averaged turbulence is concerned. This hypothesis is dictated by a recent study (Painemal et al., 2017) that infers the entrainment rate over subtropical northeast Pacific using satellite and reanalysis data based on the mass conservation equation. It shows a marked offshore decrease in entrainment rate, a spatial pattern anchoring the occurrence frequency of Cu-fed STBLs.

5. Discussion and Conclusions

This study examines the role of CTRC in regulating the surface-cloud coupling, surface LHFs, and cloud-base heights in marine boundary layers capped by extensive Sc decks. The study region is the subtropical northeast Pacific Ocean where a 6-month worth of shipborne observation made along swaths from the coast of California to the Hawaii is exploited. A distinctive feature of this study is that instead of using the degree of boundary layer mixing state for classifying STBLs into coupled and decoupled ones (Jones et al., 2011), we categorize the coupling state of the samples according to whether there are Cu feedings. Using this classification scheme, we find that the decoupled Sc decks without Cu feedings rarely occur in subtropical northeast Pacific. This is because of the prevailing equatorward flow that advects Sc decks over progressively warmer water, a large-scale condition favorable for the initiation, and vertical penetration of Cu clouds that feed moisture to the previously decoupled Sc decks. This leaves the decoupled single-layer Sc, a marginal category of cloud over the subtropical northeast Pacific, which serves as the basis for a recently developed satellite remote sensing technique that infers the decoupling degree of Sc decks from the spatial distribution of LWP (Zheng et al., 2018). In absence of the decoupled Sc decks, two STBL regimes dominate: well-mixed and Cu-coupled STBLs. The occurrence frequencies of these two STBL regimes are controlled not only by the large-scale dynamics but also by the CTRC. Well-mixed STBLs occur more frequently when the CTRC is strong.

In well-mixed STBLs, we find that the surface LHFs and cloud-base height increase with the CTRC rate via the entrainment process. Greater CTRC generates stronger turbulence and, hence, larger entrainment rate that desiccates the STBL, elevates the LCL, and promotes stronger LHFs. To what extent the surface fluxes and cloud-base height respond to the CTRC is regulated by the strength of the temperature inversion that caps

the marine boundary layer. Their responses are more sensitive in weak-inversion conditions that favor more efficient entrainment. Such an association between the CTRC and surface LHFs is not found in Cu-fed STBLs, indicating that the signature of CTRC-modulated entrainment in surface energetics is not detectable at diurnal time scale. Ship-based observations show markedly greater surface LHFs versus the CTRC in Cu-fed STBLs. This is indicative of a strong surface forcing in Cu-coupled STBLs that occur more offshore where the low-level cold temperature advection induces stronger surface LHFs than that in coastal regions (Bretherton & Wyant, 1997). The greater surface forcing substantially weakens the signature of CTRC in driving convective circulations and the surface energetics in boundary layers. We hypothesize that in the absence of low-level temperature advection, the CTRC in Cu-coupled STBLs should still play an important role in regulating the surface energetics. The time scale of the CTRC effects may be longer than that in well-mixed STBLs due to the greater depth of boundary layer and the static stability of the subcloud layer that suppresses vertical mixing. Examination of this hypothesis requires sampling Cu-coupled STBLs over regions where the low-level temperature advection is weak. A survey of the Sc clouds in middle- and high-latitude oceans may offer such samples. We plan to pursue this in the future.

Acknowledgments
The study was supported by NOAA's JPSS program and NWS program (NA15NWS4680011) and the Department of Energy's (DOE) Atmospheric System Research program (DE-SC0018996). The second author is supported by the Joint NSFC-ISF Research Program (41561144004), jointly funded by the National Natural Science Foundation of China and the Israel Science Foundation. The ground-based data in this study are available from website of ARM Climate Research Facility (www.archive.arm.gov/data). The GOES-15 cloud parameters data are obtained from the NASA Langley Cloud and Radiation Research Group (https://satcorps.larc.nasa.gov). We thank the four anonymous reviewers whose comments considerably improve the manuscript.

References

Albrecht, B. A., Bretherton, C. S., Johnson, D., Schubert, W. H., & Frisch, A. S. (1995). The Atlantic stratocumulus transition experiment—ASTEX. *Bulletin of the American Meteorological Society*, *76*(6), 889–904. https://doi.org/10.1175/1520-0477(1995)076<0889:TASTE>2.0.CO;2

Albrecht, B. A., Fairall, C. W., Thomson, D. W., White, A. B., Snider, J. B., & Schubert, W. H. (1990). Surface-based remote sensing of the observed and the adiabatic liquid water content of stratocumulus clouds. *Geophysical Research Letters*, *17*(1), 89–92. https://doi.org/10.1029/GL017i001p00089

Bohren, C. F., & Albrecht, B. A. (1998), *Atmospheric thermodynamics*. Oxford, UK: Oxford University Press.

Bretherton, C. S., & Wyant, M. C. (1997). Moisture transport, lower-tropospheric stability, and decoupling of cloud-topped boundary layers. *Journal of the Atmospheric Sciences*, *54*(1), 148–167. https://doi.org/10.1175/1520-0469(1997)054<0148:MTLTSA>2.0.CO;2

Caldwell, P., Bretherton, C. S., & Wood, R. (2005). Mixed-layer budget analysis of the diurnal cycle of entrainment in southeast Pacific stratocumulus. *Journal of the Atmospheric Sciences*, *62*(10), 3775–3791. https://doi.org/10.1175/JAS3561.1

Considine, G., Curry, J. A., & Wielicki, B. (1997). Modeling cloud fraction and horizontal variability in marine boundary layer clouds. *Journal of Geophysical Research*, *102*(D12), 13,517–13,525. https://doi.org/10.1029/97JD00261

Craven, J. P., Jewell, R. E., & Brooks, H. E. (2002). Comparison between observed convective cloud-base heights and lifting condensation level for two different lifted parcels. *Weather and Forecasting*, *17*(4), 885–890. https://doi.org/10.1175/1520-0434(2002)017<0885:CBOCCB>2.0.CO;2

Deardorff, J. (1980). Cloud top entrainment instability. *Journal of the Atmospheric Sciences*, *37*(1), 131–147. https://doi.org/10.1175/1520-0469(1980)037<0131:CTEI>2.0.CO;2

Dong, X., Schwantes, A. C., Xi, B., & Wu, P. (2015). Investigation of the marine boundary layer cloud and CCN properties under coupled and decoupled conditions over the Azores. *Journal of Geophysical Research: Atmospheres*, *120*, 6179–6191. https://doi.org/10.1002/2014JD022939

Eastman, R., Wood, R., & Bretherton, C. S. (2016). Time scales of clouds and cloud-controlling variables in subtropical stratocumulus from a Lagrangian perspective. *Journal of the Atmospheric Sciences*, *73*(8), 3079–3091. https://doi.org/10.1175/JAS-D-16-0050.1

Fairall, C., Hare, J., & Snider, J. (1990). An eight-month sample of marine stratocumulus cloud fraction, albedo, and integrated liquid water. *Journal of Climate*, *3*(8), 847–864. https://doi.org/10.1175/1520-0442(1990)003<0847:AEMSOM>2.0.CO;2

Fairall, C. W., Bradley, E. F., Rogers, D. P., Edson, J. B., & Young, G. S. (1996). Bulk parameterization of air-sea fluxes for tropical ocean-global atmosphere coupled-ocean atmosphere response experiment. *Journal of Geophysical Research*, *101*(C2), 3747–3764. https://doi.org/10.1029/95JC03205

Garreaud, R., & Muñoz, R. (2004). The diurnal cycle in circulation and cloudiness over the subtropical southeast Pacific: A modeling study. *Journal of Climate*, *17*(8), 1699–1710. https://doi.org/10.1175/1520-0442(2004)017<1699:TDCICA>2.0.CO;2

Goren, T., Rosenfeld, D., Sourdeval, O., & Quaas, J. (2018). Satellite observations of precipitating marine stratocumulus show greater cloud fraction for decoupled clouds in comparison to coupled clouds. *Geophysical Research Letters*, *45*, 5126–5134. https://doi.org/10.1029/2018GL078122

Hartmann, D. L., Ockert-Bell, M. E., & Michelsen, M. L. (1992). The effect of cloud type on Earth's energy balance: Global analysis. *Journal of Climate*, *5*(11), 1281–1304. https://doi.org/10.1175/1520-0442(1992)005<1281:TEOCTO>2.0.CO;2

Hartmann, D. L., & Short, D. A. (1980). On the use of Earth radiation budget statistics for studies of clouds and climate. *Journal of the Atmospheric Sciences*, *37*(6), 1233–1250. https://doi.org/10.1175/1520-0469(1980)037<1233:OTUOER>2.0.CO;2

Jones, C., Bretherton, C., & Leon, D. (2011). Coupled vs. decoupled boundary layers in VOCALS-REx. *Atmospheric Chemistry and Physics*, *11*(14), 7143–7153. https://doi.org/10.5194/acp-11-7143-2011

Kazil, J., Yamaguchi, T., & Feingold, G. (2017). Mesoscale organization, entrainment, and the properties of a closed-cell stratocumulus cloud. *Journal of Advances in Modeling Earth Systems*, *9*, 2214–2229. https://doi.org/10.1002/2017MS001072

Klein, S. A., Hartmann, D. L., & Norris, J. R. (1995). On the relationships among low-cloud structure, sea surface temperature, and atmospheric circulation in the summertime northeast Pacific. *Journal of Climate*, *8*(5), 1140–1155. https://doi.org/10.1175/1520-0442(1995)008<1140:OTRALC>2.0.CO;2

Lawrence, M. G. (2005). The relationship between relative humidity and the dewpoint temperature in moist air: A simple conversion and applications. *Bulletin of the American Meteorological Society*, *86*(2), 225–234. https://doi.org/10.1175/BAMS-86-2-225

Leon, D. C., Wang, Z., & Liu, D. (2008). Climatology of drizzle in marine boundary layer clouds based on 1 year of data from CloudSat and Cloud-Aerosol Lidar and Infrared Pathfinder Satellite Observations (CALIPSO). *Journal of Geophysical Research*, *113*, D00A14. https://doi.org/10.1029/2008JD009835

Lewis, E., & Teixeira, J. (2015). Dispelling clouds of uncertainty. *Eos, Transactions American Geophysical Union*, *96*. BNL--107566-2015-JA

Lilly, D. K. (1968). Models of cloud-topped mixed layers under a strong inversion. *Quarterly Journal of the Royal Meteorological Society*, *94*(401), 292–309. https://doi.org/10.1002/qj.49709440106

Martin, G., Johnson, D., Rogers, D., Jonas, P., Minnis, P., & Hegg, D. (1995). Observations of the interaction between cumulus clouds and warm stratocumulus clouds in the marine boundary layer during ASTEX. *Journal of the Atmospheric Sciences*, *52*(16), 2902–2922. https://doi.org/10.1175/1520-0469(1995)052<2902:OOTIBC>2.0.CO;2

Matsui, T., Masunaga, H., Kreidenweis, S. M., Pielke, R. A., Tao, W. K., Chin, M., & Kaufman, Y. J. (2006). Satellite-based assessment of marine low cloud variability associated with aerosol, atmospheric stability, and the diurnal cycle. *Journal of Geophysical Research*, *111*, D17204. https://doi.org/10.1029/2005JD006097

Miller, M. A., & Albrecht, B. A. (1995). Surface-based observations of mesoscale cumulus–stratocumulus interaction during ASTEX. *Journal of the Atmospheric Sciences*, *52*(16), 2809–2826. https://doi.org/10.1175/1520-0469(1995)052<2809:SBOOMC>2.0.CO;2

Minnis, P., Kratz, D. P., Coakley, J. A., King, M. D., Garber, D., Heck, P., et al. (1995). Clouds and the Earth's RadiantEnergy System (CERES) algorithm theoretical basis document: Cloud optical property retrieval (subsystem 4.3), NASA RP 1376(pp. 135–164). Retrieved from http://www-pm.larc.nasa.gov/ceres/pub/journals/Minnis.etal.95.III.pdf, (Accessed 2017/02/18).

Nicholls, S. (1984). The dynamics of stratocumulus: Aircraft observations and comparisons with a mixed layer model. *Quarterly Journal of the Royal Meteorological Society*, *110*(466), 783–820. https://doi.org/10.1002/qj.49711046603

O'Dell, C. W., Wentz, F. J., & Bennartz, R. (2008). Cloud liquid water path from satellite-based passive microwave observations: A new climatology over the global oceans. *Journal of Climate*, *21*(8), 1721–1739. https://doi.org/10.1175/2007JCLI1958.1

Painemal, D., Minnis, P., Ayers, J. K., & O'Neill, L. (2012). GOES-10 microphysical retrievals in marine warm clouds: Multi-instrument validation and daytime cycle over the southeast Pacific. *Journal of Geophysical Research*, *117*, D19212. https://doi.org/10.1029/2012JD017822

Painemal, D., Xu, K. M., Palikonda, R., & Minnis, P. (2017). Entrainment rate diurnal cycle in marine stratiform clouds estimated from geostationary satellite retrievals and a meteorological forecast model. *Geophysical Research Letters*, *44*, 7482–7489. https://doi.org/10.1002/2017GL074481

Rahn, D. A., & Garreaud, R. (2010). Marine boundary layer over the subtropical southeast Pacific during VOCALS-REx—Part 1: Mean structure and diurnal cycle. *Atmospheric Chemistry and Physics*, *10*(10), 4491–4506. https://doi.org/10.5194/acp-10-4491-2010

Stephens, G. L. (2005). Cloud feedbacks in the climate system: A critical review. *Journal of Climate*, *18*(2), 237–273. https://doi.org/10.1175/JCLI-3243.1

Stephens, G. L., & Greenwald, T. J. (1991). The Earth's radiation budget and its relation to atmospheric hydrology: 2. Observations of cloud effects. *Journal of Geophysical Research*, *96*(D8), 15,325–15,340. https://doi.org/10.1029/91JD00972

Stevens, B., Cotton, W. R., Feingold, G., & Moeng, C.-H. (1998). Large-eddy simulations of strongly precipitating, shallow, stratocumulus-topped boundary layers. *Journal of the Atmospheric Sciences*, *55*(24), 3616–3638. https://doi.org/10.1175/1520-0469(1998)055<3616:LESOSP>2.0.CO;2

Tang, F., & Zou, X. (2018). Diurnal variation of liquid water path derived from two polar-orbiting FengYun-3 microwave radiation imagers. *Geophysical Research Letters*, *45*, 6281–6288. https://doi.org/10.1029/2018GL077857

Wood, R. (2012). Stratocumulus clouds. *Monthly Weather Review*, *140*(8), 2373–2423. https://doi.org/10.1175/MWR-D-11-00121.1

Wood, R., Bretherton, C., & Hartmann, D. (2002). Diurnal cycle of liquid water path over the subtropical and tropical oceans. *Geophysical Research Letters*, *29*(23), 2092. https://doi.org/10.1029/2002GL015371

Wood, R., & Bretherton, C. S. (2004). Boundary layer depth, entrainment, and decoupling in the cloud-capped subtropical and tropical marine boundary layer. *Journal of Climate*, *17*(18), 3576–3588. https://doi.org/10.1175/1520-0442(2004)017<3576:BLDEAD>2.0.CO;2

Wood, R., Köhler, M., Bennartz, R., & O'Dell, C. (2009). The diurnal cycle of surface divergence over the global oceans. *Quarterly Journal of the Royal Meteorological Society*, *135*(643), 1484–1493. https://doi.org/10.1002/qj.451

Wood, R., Kuan-Ting, O., Bretherton, C. S., Mohrmann, J., Albrecht, B. A., Zuidema, P., Ghate, V., et al. (2018). Ultraclean layers and optically thin clouds in the stratocumulus-to-cumulus transition. Part I: Observations. *Journal of the Atmospheric Sciences*, *75*(5), 1631–1652. https://doi.org/10.1175/JAS-D-17-0213.1

Wood, R., & Taylor, J. P. (2001). Liquid water path variability in unbroken marine stratocumulus cloud. *Quarterly Journal of the Royal Meteorological Society*, *127*(578), 2635–2662. https://doi.org/10.1002/qj.49712757807

Wood, R., Wyant, M., Bretherton, C. S., Rémillard, J., Kollias, P., Fletcher, J., Stemmler, J., et al. (2015). Clouds, aerosols, and precipitation in the marine boundary layer: An arm mobile facility deployment. *Bulletin of the American Meteorological Society*, *96*(3), 419–440. https://doi.org/10.1175/BAMS-D-13-00180.1

Wyant, M. C., Wood, R., Bretherton, C. S., Mechoso, C. R., Bacmeister, J., Balmaseda, M. A., Barrett, B., et al. (2010). The PreVOCA experiment: Modeling the lower troposphere in the Southeast Pacific. *Atmospheric Chemistry and Physics*, *10*(10), 4757–4774. https://doi.org/10.5194/acp-10-4757-2010

Xiao, H., Wu, C.-M., & Mechoso, C. R. (2011). Buoyancy reversal, decoupling and the transition from stratocumulus to shallow cumulus topped marine boundary layers. *Climate Dynamics*, *37*(5–6), 971–984. https://doi.org/10.1007/s00382-010-0882-3

Zheng, Y., & Rosenfeld, D. (2015). Linear relation between convective cloud base height and updrafts and application to satellite retrievals. *Geophysical Research Letters*, *42*, 6485–6491. https://doi.org/10.1002/2015GL064809

Zheng, Y., Rosenfeld, D., & Li, Z. (2016). Quantifying cloud base updraft speeds of marine stratocumulus from cloud top radiative cooling. *Geophysical Research Letters*, *43*, 11,407–11,413. https://doi.org/10.1002/2016GL071185

Zheng, Y., Rosenfeld, D., & Li, Z. (2018). Estimating the decoupling degree of subtropical marine stratocumulus decks from satellite. *Geophysical Research Letters*, *45*. https://doi.org/10.1029/2018GL078382

Zhou, X., Kollias, P., & Lewis, E. R. (2015). Clouds, precipitation, and marine boundary layer structure during the MAGIC field campaign. *Journal of Climate*, *28*(6), 2420–2442. https://doi.org/10.1175/JCLI-D-14-00320.1

Zuidema, P., & Hartmann, D. L. (1995). Satellite determination of stratus cloud microphysical properties. *Journal of Climate*, *8*(6), 1638–1657. https://doi.org/10.1175/1520-0442(1995)008<1638:SDOSCM>2.0.CO;2

Zuidema, P., Painemal, D., De Szoeke, S., & Fairall, C. (2009). Stratocumulus cloud-top height estimates and their climatic implications. *Journal of Climate*, *22*(17), 4652–4666. https://doi.org/10.1175/2009JCLI2708.1